Advances in Geo-Energy Research

Vol. 16, No. 1, p. 60-76, 2025

Original article

Experimental study on compound dynamic disaster in deep coal rock under gas and stress loading and unloading

Xin Zhang[1], Jupeng Tang[1,2]*, Yishan Pan[1,3], Lingran Ren[1], Lei Huang[1], Zhonghua Zhang[1]

[1]*School of Mechanics and Engineering, Liaoning Technical University, Fuxin 123000, P. R. China*

[2]*School of Environment, Shenyang University, Shenyang 110044, P. R. China*

[3]*Institute of Disaster Rock Mechanics, Liaoning University, Shenyang 110036, P. R. China*

Keywords:
Deep mining
true triaxial tests
compound dynamic disaster
gas and stress loading and unloading
transformation mechanism

Cited as:
Zhang, X., Tang, J., Pan, Y., Ren, L., Huang, L., Zhang, Z. Experimental study on compound dynamic disaster in deep coal rock under gas and stress loading and unloading. Advances in Geo-Energy Research, 2025, 16(1): 60-76.
https://doi.org/10.46690/ager.2025.04.07

Abstract:
To explore the occurrence mechanism of compound dynamic disasters in coal rocks, this study conducted a true triaxial test simulating gas extraction and stress loading and unloading conditions. To differentiate behaviors among disaster types, the effects of acoustic emission energy, temperature and impact force were analyzed during disaster incubation. The results revealed that different simulation depths lead to varying types of compound dynamic disasters. Compared to rockburst-outburst compound dynamic disasters, outburst-rockburst compound dynamic disasters exhibited higher relative outburst intensity and critical gas pressure. Deep coal rock disasters were characterized by long incubation and short excitation. As a threshold for disaster type transformation, a critical gas pressure range of 2.2-2.8 MPa was identified. During incubation, the temperature generally increased, with greater variation in the coal seam than at the coal-rock interface. During excitation, the temperature dropped sharply, with smaller variation in the coal seam. Outburst-rockburst disasters consistently showed higher temperature variation than rockburst-outburst disasters. Impact force evolution in roadways followed a similar pattern across disaster types: initial impact → intensification → peak → attenuation, with a peak effect. The peak impact force increased linearly with critical gas pressure, with outburst-rockburst peak growth rates being 47.76 times higher than rockburst-outburst peak growth rates. This study provides important insights into the multi-parameter evolution characteristics of deep coal rock compound dynamic disasters, offering a scientific basis for disaster prediction and control.

1. Introduction

Coal is a significant resource in China, accounting for 55.3% of the country's total energy consumption in 2023. However, many dynamic disasters have occurred in the underground coal mining process (Díaz Aguado and González Nicieza, 2007; Chen et al., 2012; Zhou et al., 2018a). Coal and gas outbursts, along with rockbursts, represent two of the most common dynamic disasters encountered in coal mining operations (Xue et al., 2011; Jiang et al., 2012; Qiu et al., 2023). Coal and gas outburst is an extremely complex mine gas dynamic phenomenon encountered in coal mine production, in which a large amount of coal is suddenly thrown out from the coal body to the roadway or mining space in a very short time along with a large amount of gas (Li et al., 2015; Xu and Jiang, 2017; Zhang et al., 2022a). Rockburst occurs when coal and the surrounding rock are in a state of high stress and the accumulated elastic deformation energy is suddenly released under the effect of external disturbance, leading to sudden and drastic destruction, collapse or ejection of the coal rock. This phenomenon is usually accompanied

*Corresponding author.
E-mail address: LntuZx0812@163.com (X. Zhang); tangjupeng@lntu.edu.cn (J. Tang); panyish_cn@sina.com (Y. Pan); 47221007@stu.lntu.edu.cn (L. Ren); 13899014189@163.com (L. Huang); 15660115826@163.com (Z. Zhang).
2207-9963
Received January 18, 2025; revised February 15, 2025; accepted March 10, 2025; available online March 17, 2025.

Yandy Scientific Press

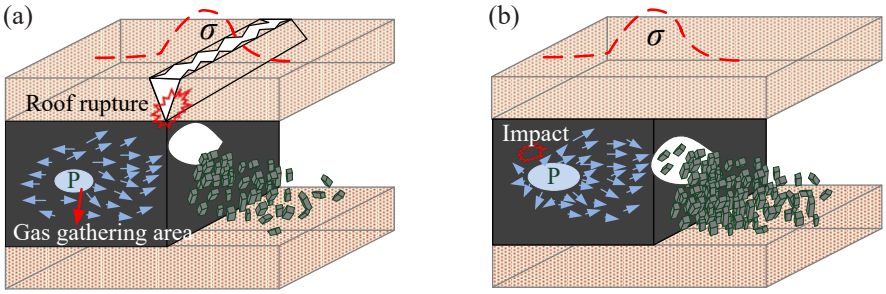

Fig. 1. Schematic diagram of two compound dynamic disaster occurrence modes: (a) Rockburst-outburst compound dynamic disaster and (b) outburst-rockburst compound dynamic disaster.

by violent vibrations, loud noise and gas waves (Konicek et al., 2013; Dong et al., 2020).

In the past decades, numerous academics have extensively studied the mechanism, prediction and prevention measures of coal and gas outburst and rockburst and made significant achievements (Tang et al., 2022; Li et al., 2023; Soleimani et al., 2023; Wang et al., 2024). The mining depth is currently growing by 10∼25 m/year, with the majority of coal mines now operating beyond 1,000 m and some exceeding depths of 1,500 m (Xie et al., 2019). However, the interaction between the two dynamic disasters began to emerge and intensify after the commencement of deep mining, displaying a compound occurrence of the two dynamic disasters (Zhang et al., 2019). In China, such events are often referred to as compound dynamic disasters (Lu et al., 2020a). They may be mutually induced, mutually strengthened, or produce a resonance effect in the process of disaster incubation, occurrence and development (Zhao and Jiang, 2010; Wei et al., 2018). Compound dynamic disasters possess both the characteristics of coal and gas outburst and rockburst, making them difficult to classify the accidents as a single mine dynamic disaster type (Dong et al., 2020). The intensity of the latter disasters once they occur is greater and more violent, easily leading to sudden major disasters and accidents (Li et al., 2007, 2021; Hu et al., 2015). For example, the Sunjiawan Coal Mine's "2·14" incident, the rockburst induced a serious gas explosion, resulting in 214 deaths and 30 injuries. In the Pingdingshan Coal Mine, the "6·29" and "11·12" incidents involved a rockburst triggering coal and gas outburst accidents. The Xinyi Coal Mine's "7·11" incident saw a floor faulting-induced rockburst that triggered a coal and gas outburst. In the Yangou Coal Mine, the "11·8" incident involved a particularly large coal and gas outburst during rock cross-cut coal uncovering, which induced a floor rockburst, leading to 2 deaths and 1 injury (Wang et al., 2016; Zhu et al., 2018). Therefore, investigating compound dynamic disasters in deep coal rock through experimental research is crucial to better understand disaster mechanisms and enhance the prediction, prevention and control capabilities.

Petukhov (1983) initially introduced the idea of a unified approach to studying rockburst and coal and gas outburst, highlighting the need for a unified theory. Subsequently, Zhang et al. (1991) put forward the unified instability theory of rockburst and coal and gas outburst on the basis of the deformation and failure mechanism of coal rock. According to this theory, both rockburst and coal and gas outburst are dynamic instability processes that occur when the coal rock deformation system is disturbed under the condition of unstable equilibrium. However, the occurrence of coal and gas outburst is affected by gas, in contrast to rockburst that ignores the effect of gas. However, the above model did not consider the factors of mutual transformation and mutual induction between rockburst and coal and gas outburst. Since then, an increasing number of scholars have reproduced the evolution process of dynamic disasters through laboratory experiments, theoretical analysis and numerical simulations, studying the occurrence mechanism, prediction, early warning, and prevention of compound disasters (Dou et al., 2014; Zhou et al., 2019). Lu et al. (2020b) carried out extensive experimental research and found that the occurrence process of coal and gas compound dynamic disasters exhibits distinct stages and precursors. Wang et al. (2025) established a compound disaster energy equation that takes into account the influence of the elastic energy of the roof, derived a disaster energy criterion considering the effect of the roof's elastic energy, and introduced COMSOL to conduct numerical simulations of coal seam mining under different *in-situ* stresses and gas pressures. The research results indicated that stress conditions are crucial to the occurrence of dynamic disasters and that the gas effect cannot be neglected. Furthermore, many scholars have classified the types of compound dynamic disasters (Shepherd et al., 1981; Wang and Du, 2019), among which two widely recognized types are rockburst-outburst compound dynamic disasters and outburst-rockburst compound dynamic disasters. Their occurrence modes are shown in Fig. 1.

In summary, deep coal rock compound dynamic disasters have emerged as a critical challenge hindering the safe and efficient extraction of coal resources. These incidents are influenced by various factors, including *in-situ* stress, gas pressure, and the mechanical characteristics of coal rock, with intricate mechanisms and development processes (Sobczyk, 2011; Xue et al., 2016; Yang et al., 2019; Zhang et al., 2022b). While prior research has provided foundational insights into the mechanisms behind coal and gas compound dynamic disasters, there is a notable gap in studies that treat gas-containing coal rock structures as integrated systems. Specifically, there has been limited systematic investigation into the mechanisms of compound dynamic disasters triggered by the coupled instability of coal, rock and gas during loading processes.

Furthermore, the differences in the behavior of Acoustic Emission (AE) energy, temperature and post-disaster impact force during the incubation of different compound dynamic disasters have not been explored.

In this research, a true triaxial apparatus was employed to perform a series of experiments on compound dynamic disasters at various simulated depths. The incubation and excitation processes of these disasters were monitored using an acoustic emission system. The evolution of coal rock temperature, roadway impact force, and the intensity of different compound dynamic disasters were systematically examined. Furthermore, the conditions under which these disasters induce and transform into each other were investigated along with the underlying mechanisms. The findings are crucial for enhancing our understanding of the mechanisms of compound dynamic disasters and enhancing the prediction and prevention strategies.

2. Experimental methodology

2.1 Model similarity

In physical simulation experiments, it is crucial to maintain a high level of consistency between the model and the prototype in the studied physical processes. The similarity of two physical phenomena encompasses multiple dimensions, including geometric, kinematic and dynamic similarities. Earlier experimental research primarily emphasized similarity in the following areas (Skoczylas, 2012, 2014; Cao et al., 2019; Geng et al., 2020):

(1) Mechanical similarity

According to the similarity theorems, the outburst coal mass can be approximately regarded as a stage-wise linear elastomer. By applying the equation analysis method to perform similarity transformations on the fundamental equations of elasticity, corresponding similarity index equations can be obtained.

Taking the equilibrium equation as a basis, the similarity criterion considering body forces K_1 is (Nie et al., 2019):

$$K_1 = \frac{\sigma}{L\gamma} = c \tag{1}$$

where σ represents the stress, MPa; L represents the length, m; γ represents the bulk density, kg/m^3; c is a constant.

Thus, the similar index C_1 is obtained, that is:

$$C_1 = \frac{C_\sigma}{C_L C_\rho} = 1 \tag{2}$$

where C_σ represents the stress similarity constant, C_L represents the geometric similarity constant, and C_ρ is the body force similarity constant.

The similar index C_2 is obtained from geometric equations, namely:

$$C_2 = \frac{C_\varepsilon C_L}{C_S} = 1 \tag{3}$$

where C_ε represents the strain similarity constant, and C_S represents the displacement similarity constant.

The similar indexes C_3 and C_4 can be obtained from the constitutive equation, namely:

$$C_3 = \frac{C_S C_E}{C_\sigma} = 1 \tag{4}$$

$$C_4 = \frac{C_\varepsilon C_E}{C_\mu C_\sigma} = 1 \tag{5}$$

where C_E represents the elastic modulus similarity constant, and C_μ represents the Poisson's ratio similarity constant.

(2) Kinematic similarity

Next, the kinematic similarity ratio of the test models needs to be examined, which mainly includes two aspects: velocity similarity and acceleration similarity.

Velocity similarity (Nie et al., 2019):

$$C_v = \frac{v_p}{v_m} \tag{6}$$

where C_v represents the velocity similarity constant; v_p represents the prototype velocity, m/s; v_m represents the model velocity, m/s. Substituting and cancelling the time parameter yields $C_v = \sqrt{C_L}$.

Acceleration similarity:

$$C_a = \frac{a_p}{a_m} \tag{7}$$

where C_a represents the acceleration similarity constant; C_t represents the time similarity constant; a_p represents the prototype acceleration, m/s^2; a_m represents the model acceleration, m/s^2. Substituting and cancelling the time parameter yields $C_a = C_v/C_t$.

(3) Unsteady similarity

The coal-gas two-phase flow is unsteady, and its motion state is changing all the time in the roadway, therefore it is necessary to ensure the similarity of its motion with time (Jin et al., 2018). The unsteady similarity of the model can be tested by the Strouhal number:

$$\frac{Sr_p}{Sr_m} = \frac{\dfrac{L_p}{v_p t_p}}{\dfrac{L_m}{v_m t_m}} = \frac{\dfrac{L_p}{L_m}}{\dfrac{v_p t_p}{v_m t_m}} = \frac{C_L}{C_v C_t} = \frac{C_L}{\sqrt{C_L}\sqrt{C_L}} = 1 \tag{8}$$

where L_p represents the prototype length, m; L_m represents the model length, m; t_p represents the prototype time, s; t_m represents the model time, s; Sr_p represents the Strouhal number in the prototype; Sr_m represents the Strouhal number in the model.

The test results meet the requirements, so the designed model can be used to simulate the motion characteristics of coal-gas two-phase flow.

2.2 Sample preparation

The test coal samples were selected from the Pingdingshan Coal Mine in Henan Province, central-eastern China, which is a compound dynamic disaster mine. It is of great engineering significance to choose these coal samples as the research object. Due to challenges in acquiring large quantities of raw coal, briquette samples were utilized, a common practice in investigating coal mine dynamic disasters (Wang et al., 2018; Zhang et al., 2021). Firstly, raw coal lumps were manually broken down into smaller fragments, followed by mechanical crushing to achieve finer particles. Various particle sizes were

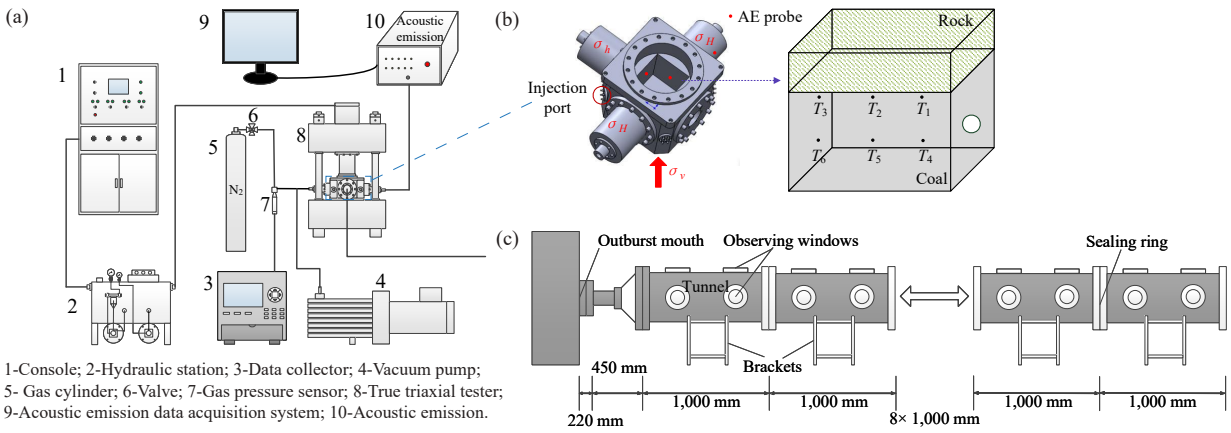

Fig. 2. True triaxial coal rock compound dynamic disaster simulation test device. (a) Schematic diagram of test device, (b) sensors layout and (c) roadway.

Table 1. Ratio scheme of briquette.

Particle size (mesh)	Particle size (mm)	Mass ratio (%)
20∼40	0.425∼0.85	29.3
40∼60	0.25∼0.425	16.5
60∼80	0.18∼0.25	8.2
80∼100	0.15∼0.18	4
> 100	0∼0.15	42

then separated through sieving. Studies have indicated that briquettes produced by crushing non-structural coal to specific particle sizes and compacting them at defined ratios exhibit mechanical strength, adsorption and desorption characteristics comparable to those of natural structural coal (Skoczylas et al., 2014; Yuan, 2016).

At present, there is no uniform regulation on the proportion of briquette in laboratory tests. Therefore, on the basis of previous research experience (Zhang et al., 2022a), this paper carries out the proportion of briquette building on the theory of maximum density curve. The maximum density curve is an ideal curve proposed by Fuller through experiments. It is considered that solid particles are arranged regularly according to particle size, and the density can be maximized and the pores are minimized. As a result, briquette specimens with physical and mechanical properties similar to those of raw coal are obtained. The relevant expression is:

$$Q = \sqrt{\frac{d}{D}} \times 100\% \tag{9}$$

where Q represents the passing percentage of the required pulverized coal particle size, %; d represents the required pulverized coal particle size, mm; D is the maximum particle size of pulverized coal, mm.

The coal powder particle size is screened into five intervals of 20∼40, 40∼60, 60∼80, 80∼100, and > 100 mesh. According to Eq. (9), the final proportions are shown in Table 1, where the > 100 mesh part contains 5% cement binder. After conducting a lot of tests, it is found that the rock samples with a sand cement: water mass ratio of 8:5:1 meet the test requirements. The average water content of different particle size ranges is measured to be 1.148 %. To make the briquette bond better, part of water was added to the test to make the water content of the briquette reach 2%, and the proportioned coal powder was sealed and stored for the test. Considering the safety of laboratory tests, nitrogen was selected instead of methane for testing (Sobczyk, 2014; Yang et al., 2021).

2.3 Test system and scheme

In this study, a self-developed true triaxial coal rock compound dynamic disaster simulation test device was designed, as shown in Fig. 2. The test system is mainly composed of *in-situ* stress loading system, hydraulic control system, gas pressure loading system, straight roadway system, impact force monitoring system, and other acquisition and control systems.

The *in-situ* stress loading system includes a load console, press, hydraulic oil cylinder, and connecting pipeline. The cavity size is 200 mm × 200 mm × 200 mm, which supports a maximum loading pressure of 25 MPa. The system has 24 sensor interfaces, including for gas injection, acoustic, electrical, force, and thermal sensors. An 80 mm diameter outburst mouth is located at the front, with a plexiglass baffle simulating a weak surface to induce disasters. The roadway system consists of straight roadways, supports and observing windows (Fig. 2(c)) connected by 24 sections, each 1,000 mm long, with a rectangular cross-section of 200 mm × 200 mm. Sensor mounting holes are placed on the right side of the roadway for future research on the migration monitoring of two-phase flow in the roadway. The impact force is monitored using a TP-1MP voltage-type overpressure sensor with a 1,000 Hz sampling frequency and 200 K sampling length, and is triggered manually. The temperature is measured with a PT100 platinum resistor. The acoustic emission probe and temperature sensor are positioned as shown in Fig. 2(b).

Research has indicated that the emergence of compound dynamic disasters is primarily associated with roof-coal inter-

Table 2. Initial stress loading scheme.

Depth (m)	*In-situ* stress (MPa)			Test stress (MPa)		
	σ_H	σ_h	σ_v	σ'_H	σ'_h	σ'_v
1,000	48.94	28.29	26.91	4.01	2.32	2.24
1,200	58.72	33.81	32.29	4.82	2.77	2.69
1,400	68.5	39.33	37.67	5.62	3.22	3.14
1,600	78.28	44.85	43.05	6.42	3.68	3.59
1,800	88.06	50.37	48.43	7.22	4.13	4.04
2,000	97.84	55.89	53.81	8.02	4.58	4.49

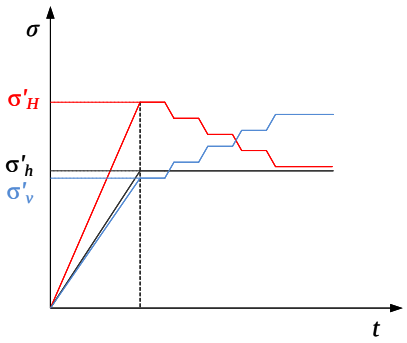

Fig. 3. Schematic diagram of stress loading.

actions, whereas coal-floor interactions are less frequently linked to such incidents. In addition, considering the size of the triaxial pressure chamber of the testing machine, if the designed rock strata are too many or too thick, this will lead to the thinning of the coal seam and thus affect the test results. Therefore, this paper establishes a coal seam-roof combination model to conduct physical simulation tests for the whole process of compound dynamic disaster manifestation under different depths in deep mines.

On the basis of the actual thickness ratio of coal seam to roof, the thickness of roof and coal seam is designed to be 40 and 160 mm, respectively, and the coal and rock mass are 8 and 4 kg, respectively. The density of briquetted coal and briquetted rock is 1,250 and 2,500 kg/m^3, respectively. According to the similarity theory and coal mine parameters, coal is taken as the object for calculation. It can be known that C_ρ is 1.032, C_L is 11.8, C_σ is 12.2, and C_p is 1. Cai et al. (2013) measured the *in-situ* stress in Pingdingshan mining as shown in:

$$\begin{aligned} \sigma_H &= 0.04 + 0.0489H \\ \sigma_h &= 0.69 + 0.0276H \\ \sigma_v &= 0.01 + 0.0269H \end{aligned} \tag{10}$$

where σ_H, σ_h and σ_v represent the maximum horizontal principal stress, minimum horizontal principal stress, and vertical principal stress, respectively, MPa; H is depth, m. After calculation, the specific initial stress loading scheme is shown in Table 2.

The specific test steps are as follows:

1) Sample pressing: Raw coal sampling → crushing → screening → determination of water content → proportioning → pressing (Zhang et al., 2022a).
2) Plexiglass baffle installation: Fit an acrylic glass plate with a sealing ring in the outburst mouth by extruding it in direct contact with the coal surface to simulate outburst weak face.
3) Tightness checking: Connect each operating system to check the air tightness of the pressure chamber. If the result is good, carry out the next test, otherwise continue to check the airtightness.
4) Vacuum and inflatable adsorption: Evacuate the triaxial pressure chamber for about 3 h to make the vacuum reach -0.1 MPa. Then, inject nitrogen to simulate pore pressure adsorption for 24 h.
5) Stress and gas pressure loading: The initial stress loading scheme is shown in Table 2. According to the Specification of Coal and Gas Outburst Prevention in China, the critical gas pressure is 0.74 MPa. Therefore, the minimum gas pressure is set to 0.6 MPa. Firstly, each stage is loaded with 0.2 MPa increments up to 1 MPa and stabilized for 2 min at each stage. Then, to simulate the gas extraction, drainage is performed on each system to make the gas pressure of 0.5 MPa or less and stabilized for 2 min. After gas extraction, horizontal unloading axial loading are performed to simulate the dynamic change of the support pressure in front of the working face during mining, with each level of unloading being 0.5 MPa and stabilized for 2 min. Subsequently, the gas pressure is set at 0.2 MPa per level, as shown in Fig. 3. This cycle is repeated until the disaster occurs and the test is completed.
6) Data collection and collation: Save and extract the data measured by the acoustic emission monitor, impact force monitoring equipment and data acquisition instrument in the whole process of coal rock compound dynamic disaster.
7) Repeat the test: Repeat the above steps, replace the initial three-dimensional stress, and carry out the next set of tests. To avoid chance events, repeat each set of tests three times.

Table 3. Test results under different simulation depths.

Depth (m)	Critical gas pressure (MPa)	Average (MPa)	Absolute outburst intensity (kg)	Average (kg)	Relative outburst intensity (%)	Average (%)	Peak impact force (MPa)	Average (MPa)	Farthest throw distance (m)
1,000 (Rockburst-outburst)	1.803	1.793	5.794	5.961	48.29	49.68	0.0672	0.0675	11.49
	1.737	1.793	6.228	5.961	51.91	49.68	0.0692	0.0675	11.49
	1.839	1.793	5.861	5.961	48.85	49.68	0.0661	0.0675	11.49
1,200 (Rockburst-outburst)	2.032	2.047	7.036	7.072	54.90	55.18	0.0711	0.0706	11.53
	2.006	2.047	7.226	7.072	56.38	55.18	0.0713	0.0706	11.53
	2.103	2.047	6.954	7.072	54.26	55.18	0.0694	0.0706	11.53
1,400 (Outburst-rockburst)	2.821	2.829	8.418	8.436	70.15	70.30	0.0955	0.0976	> 13.45
	2.811	2.829	8.531	8.436	71.09	70.30	0.1035	0.0976	> 13.45
	2.855	2.829	8.359	8.436	69.66	70.30	0.0938	0.0976	> 13.45
1,600 (Outburst-rockburst)	2.816	2.824	7.649	7.747	70.15	64.56	0.0938	0.0926	> 13.45
	2.825	2.824	8.033	7.747	71.09	64.56	0.0944	0.0926	> 13.45
	2.831	2.824	7.559	7.747	69.66	64.56	0.0896	0.0926	> 13.45
1,800 (Rockburst-outburst)	2.135	2.120	6.995	6.835	58.29	56.96	0.0698	0.0730	11.55
	2.096	2.120	6.761	6.835	56.34	56.96	0.0737	0.0730	11.55
	2.129	2.120	6.749	6.835	56.24	56.96	0.0755	0.0730	11.55
2,000 (Outburst-rockburst)	2.828	2.815	7.595	7.476	63.80	62.80	0.0905	0.0876	> 13.45
	2.816	2.815	7.569	7.476	63.58	62.80	0.0844	0.0876	> 13.45
	2.801	2.815	7.264	7.476	61.02	62.80	0.0879	0.0876	> 13.45

2.4 Experimental phenomena

At present, the professional description terms of outburst-rockburst compound dynamic disaster phenomenon have not been unified, hence the following description still refers to coal and gas outburst. Using our self-developed true triaxial test system, a series of compound dynamic disaster induction tests with different simulation depths were carried out. The gas-bearing coal rock system was subjected to extrusion deformation and failure under the coupling effect of adsorption and desorption and the mining disturbance. When the gas pressure in the cavity reached a critical value, the coal rock mass became unstable. The outburst weak surface baffle was destroyed, and the gas entrained coal dust and crushed rock particles were ejected from the outburst mouth, indicating the occurrence of a dynamic disaster. The test results under different simulation depths are shown in Table 3. Average values were used for subsequent analysis.

Following the disaster, several phenomena could be observed such as the destruction shape of holes, the quality and distribution of coal rock, the degree of crushing, the throwing distance, the transportation characteristics, sorting and dynamic manifestation. Meanwhile, the deformation and damage characteristics of coal seam roof were studied. Following Pan et al. (2024)'s research, this paper regards 1,000, 1,200, and 1,800 m as rockburst-outburst compound dynamic disasters, and 1,400, 1,600, and 2,000 m as outburst-rockburst compound dynamic disasters.

For the rockburst-outburst compound dynamic disaster, the ejection of broken coal rock mass forms a large empty roof area, as shown in Fig. 4(a), which is prone to cause large-scale collapse and caving of hard roof strata, and then induce roof fracture-type rockburst. Many broken rock blocks accumulate in the cavity. Due to the low critical gas pressure, a small number of small rock blocks are dragged into the first roadway under the action of gas pressure (Fig. 4(c)), and the ejection distance of coal rock is relatively short.

The process of outburst-rockburst compound dynamic disaster is roughly the same as the coal and gas outburst phenomenon. When the disaster occurs, the coal samples are strongly sprayed out radially under high gas pressure, accompanied by a huge sound. The outburst intensity and speed are extremely high. The strong shock wave during the outburst causes a small depression in the roof strata above the

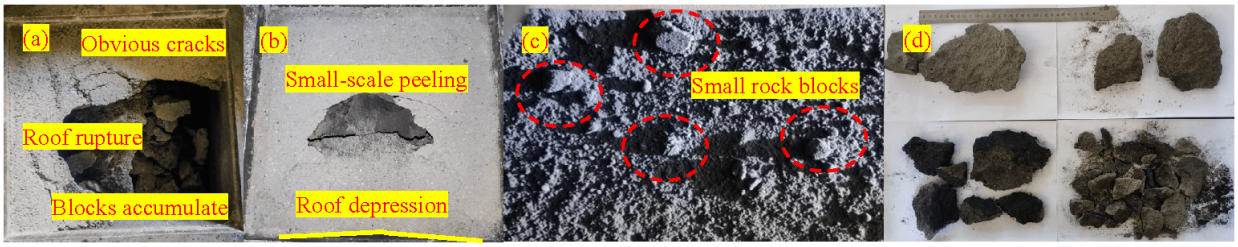

Fig. 4. Dynamic disaster phenomena. (a)-(b) Roof fracture pattern, (c) roadway coal rock distribution and (d) Fragmentation of coal rock.

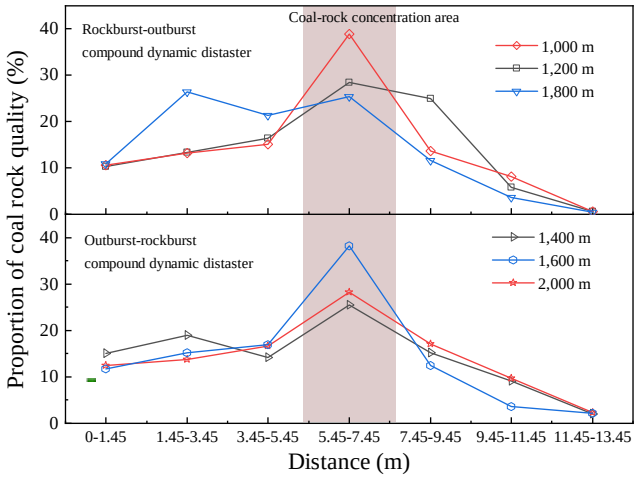

Fig. 5. Distribution characteristics of coal rock.

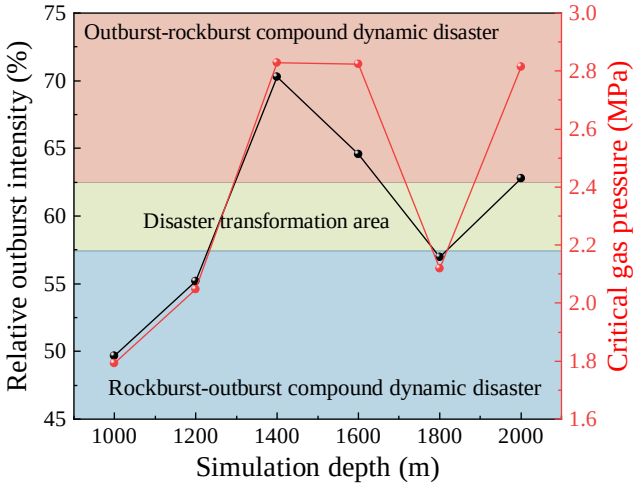

Fig. 6. Relative outburst intensity and critical gas pressure under different simulation depths.

outburst mouth, and a small-scale peeling occurs at the central position (Fig. 4(b)). The destroyed outburst weak surface is ejected along the simulated roadway, and its outburst distance is far beyond the farthest outburst distance of coal powder. The coal powder collection bags located at the roadway's end are drawn into the tunnel, a behavior consistent with earlier experimental observations (Zhang et al., 2022a). This indicates that both coal dust and gas move rapidly through the tunnel, compressing the air ahead and creating a negative pressure effect. The presence of this negative pressure is further supported by the development of impact forces, which is discussed in Section 3.4.

3. Results and analysis

3.1 Distribution and strength characteristics of coal rock

The outburst coal rock mass exhibits a decreasing characteristic and the energy gradually attenuates during the outburst process. As shown in Fig. 5, the ejected coal rock mass of tests is mainly concentrated in the range of 5.45∼7.45 m. As the ejection distance increases, the proportion of coal rock mass decreases gradually. However, the coal rock distribution characteristics of the two different types of disaster are not the same. The distribution of rockburst-outburst does not show obvious sorting and transportation characteristics, the mass of coal rock in 11.45∼13.15 m is less than 1%, and the farthest throw distance is 11.55 m. The coal rock concentration areas of the three groups are different, namely 5.45∼9.45 m, 5.45∼7.45 m and 1.45∼7.45 m, respectively. On the contrary, the outburst-rockburst coal rock distribution exhibits obvious sorting and transportation characteristics and the throwing distance is far, that is, greater than 13.45 m. In the range of 0∼5.45 m, the coal rock is distributed evenly, accounting for 11.7%∼18.9% of the total mass, and the distribution characteristics of the three groups of different simulation depths are similar. As the throwing distance increases (> 7.45 m), the mass proportion of coal rock gradually decreases. During excitation, significant adsorbed gas is released and then migrates deeper, driving coal rock movement. When the gas is completely desorbed, the gas expansion energy provided is not sufficient to transport the coal rock mass, and the outburst terminates. Throughout this process, the energy gradually attenuates.

The coal rock relative outburst intensity and critical gas pressure curves under different simulation depths are shown in Fig. 6. With the increase in simulation depth, the relative outburst intensity and critical gas pressure show an overall "N" trend. When the simulation depths are 1,000, 1,200 and 1,800 m, the relative outburst intensity and critical gas pressure are at a relatively low level, that is, 49.68%, 55.18%, 56.96% and 1.793, 2.047, 2.120 MPa, respectively. Large-scale collapse occurs in the roof strata because the outburst of the coal seam under the combined action of gas pressure, *in-situ* stress and mining stress leads to the instability of the entire system. This in turn triggers the rockburst of the roof, resulting in

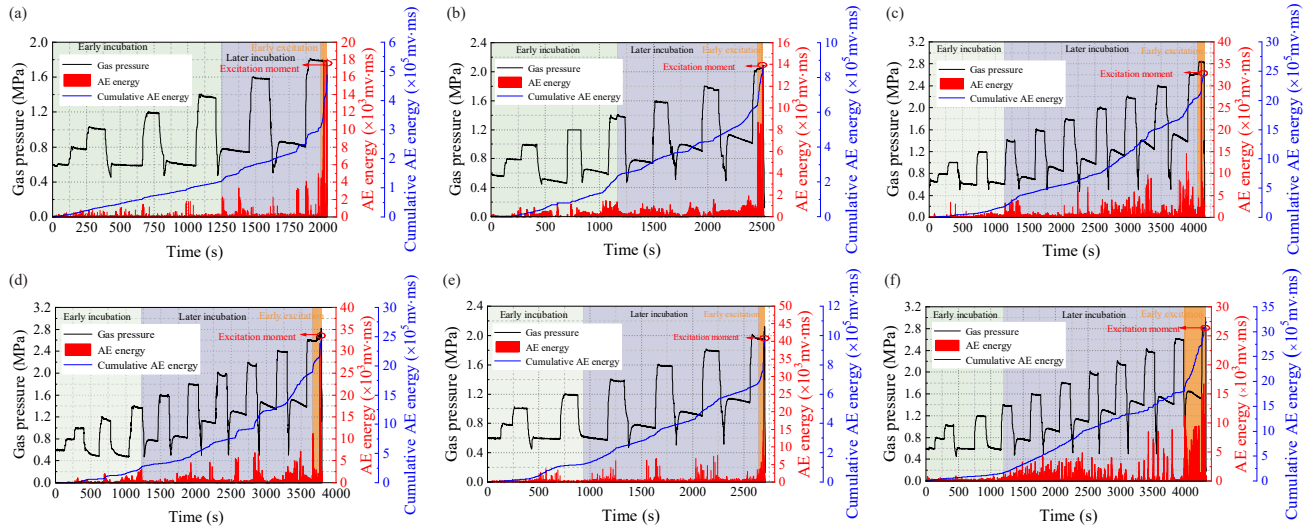

Fig. 7. Evolution characteristics of AE energy under different simulation depths. (a) 1,000 m, (b) 1,200 m, (c) 1,400 m, (d) 1,600 m, (e) 1,800 m and (f) 2,000 m.

a rockburst-outburst compound dynamic disaster. The roof extends and becomes damaged from the outburst mouth to the right rear, and the collapsed rock blocks piles up in the cavity. There are many cracks on the surface of the non-collapsed roof, and the roof may be further damaged along the cracks when subsequent disturbances occur. When the simulation depths are 1,400, 1,600 and 2,000 m, the relative outburst intensity and critical gas pressure are at relatively high levels, namely 70.3%, 64.56%, 62.8% and 2.829, 2.824, 2.815 MPa, respectively. However, there is no large-area collapse of the roof strata and only small-area peeling occurs. After the outburst, the coal seam exhibits the characteristics of small mouth and large cavity, and an outburst-rockburst compound dynamic disaster takes place. This compound dynamic disaster is dominated by outburst, and small impact disturbances cause many cracks in coal rock masses, providing structural conditions for the desorption and expansion of gas. The elastic energy of external inflow provides the energy conditions for the gas to relieve the constraints of coal rock mass. The energy released during gas desorption and expansion drives the further breakdown of coal rock, supplying both energy and transport mechanisms for the ejected material, and potentially triggering coal and gas outbursts. Consequently, the disaster's behavior and features resemble those of typical coal and gas outbursts. The intensity of the outburst shows a strong relationship with the critical gas pressure, suggesting that gas expansion energy is the primary force behind coal rock movement during the disaster initiation phase.

The test results indicate that the type of compound dynamic disaster has minimal correlation with coal seam depth: Whether at shallower depths (1,000, 1,200, 1,400 m) or greater depths (1,600, 1,800, 2,000 m), either of the two disaster types can occur. The disaster type is primarily influenced by the stress conditions, gas pressure and the coal seam's physical properties. After the coal seam enters deep mining, compared with single coal and gas outbursts and rockburst accidents, the intensity of coal rock compound dynamic disasters is greater, the critical gas pressure is lower, and low-index disaster accidents often occur.

3.2 Evolution characteristics of AE energy

The essence of the incubation, occurrence and development of compound disasters in deep coal rock is a multi-scale competitive evolution process in which the gas expansion energy and coal rock deformation energy are accumulated microscopically, manifested macroscopically, and released in the scale of engineering under the solid-gas coupling effect of human mining-induced gas and coal. During this period, the two types of energy compete and accumulate. AE monitoring enables the acquisition of extensive data on deformation and damage within coal bodies, precisely detecting the micro-fracture events associated with coal rock mass instability. Given the unclear mechanisms behind deep coal rock compound dynamic disasters, this study conducted research on the AE energy evolution during coal fracture across various simulated depths, holding significant practical value for the effective prediction and prevention of such disasters in coal mines.

Taking the theory of Mechanical Mechanism of Coal and Gas Outburst proposed by Hu et al. (2015) and the change of AE energy amplitude with time as bases, the incubation of coal rock compound dynamic disasters can be divided into two stages: Early incubation and later incubation, while the excitation stage is divided into the early excitation and excitation moment. In this study, the characteristics of disaster incubation, incubation time, gas pressure, and AE energy parameters under different simulation depths were analyzed.

On the basis of the collected AE signal data, Table 4 and Fig. 7 are obtained after processing. By comparing and analyzing the test results of different simulation depths of compound dynamic disasters, the following rules are set forth:

1) The compound dynamic disaster of deep coal rock exhibits the typical characteristics of long incubation

Table 4. AE signal parameters.

Depth (m)	t_1 (s)	t_2 (s)	t_3 (s)	E_1 (10^5 mv·ms)	E_2 (10^5 mv·ms)	E_3 (10^5 mv·ms))	K_1	K_2	K_3	K_2/K_1	K_3/K_2
1,000	1,271	713	43	1.339	3.078	4.516	105.37	243.95	3,342.45	2.32	13.70
1,200	1,154	1,303	51	2.204	6.433	8.492	190.94	324.61	4,035.58	1.70	12.43
1,400	1,144	2,911	101	1.843	20.536	24.507	161.15	642.13	3,931.78	3.98	6.12
1,600	1,212	2,448	133	2.557	18.967	24.824	210.96	670.31	4,403.31	3.18	6.57
1,800	921	1,696	86	1.206	6.628	9.686	130.97	319.71	3,555.16	2.44	11.12
2,000	1,189	2,801	319	1.601	18.819	31.545	134.69	614.69	3,989.31	4.56	6.49

Notes: t denotes time, E denotes cumulative AE energy, K denotes the cumulative AE energy growth rate, and the subscripts 1, 2 and 3 represent early incubation, later incubation and early excitation, respectively.

and short excitation. The incubation and excitation time of rockburst-outburst compound dynamic disaster are shorter than those of outburst-rockburst compound dynamic disaster. As the simulation depth increases, the incubation time gradually decreases, while the early excitation time gradually increases. For different types of compound dynamic disasters, with the increase in simulation depth, the initial *in-situ* stress gradually increases, and the initial damage of coal rock masses under high *in-situ* stress is obvious. Since the critical gas pressure is relatively low when a rockburst-outburst compound dynamic disaster occurs, the incubation time gradually increases. In contrast, the incubation time of outburst-rockburst compound dynamic disasters gradually decreases. However, the early excitation time increases with the increase in simulation depth, indicating that the precursor time of deep compound dynamic disasters is longer. Before the occurrence of these disasters, the AE signals of coal rock become active, and appropriate warnings can be issued in time.

2) The AE energy undergoes an evolution process of stationary → rising → peak. In the early incubation stage, the AE energy remains fluctuating at a low level, indicating that under the effects of gas pressure loading and extraction, as well as stress loading and unloading, the coal body has experienced the formation and expansion of multiple micro-cracks. *In-situ* stress provides a prerequisite for the occurrence of disasters, while the increase in gas pressure provides power for coal ejection. Similar to the coal and gas outburst process, compound dynamic disasters also experience four stages: early incubation, later incubation, excitation-development, and termination. This shows that coal rock compound dynamic disaster is a mechanical process involving the failure of coal rock masses and energy accumulation and release. In the early excitation stage, the AE energy fluctuates abnormally and continues to rise, reaching its maximum value at the moment of excitation, which leads to a sudden release of deformation energy and gas expansion energy.
3) Analyzing the gas pressure evolution curve in Fig. 7, during the stabilization process after gas extraction, the gas pressure first increases and then decreases. With the loading and unloading of stress, the gas pressure continues to decrease. This is because after gas extraction, the initial gas adsorbed in the coal seam desorbs, resulting in a slight increase in gas pressure. When the gas pressure is balanced, the coal continues to adsorb gas, leading to a decrease in gas pressure. During the stress disturbance stage, cracks and fractures are generated in the coal, the specific surface area increases, and the coal adsorption capacity is enhanced. Since the desorption critical value has been reached, the desorption capacity is weakened, and the adsorption rate is greater than the desorption rate, so the gas pressure shows a continuous downward trend, and the greater the gas pressure before drainage is, the greater the decrease.

According to Table 4 and Fig. 8, the cumulative AE energy of outburst-rockburst compound dynamic disasters is greater than that of rockburst-outburst compound dynamic disasters. Under different simulation depths, the cumulative AE energy in the early incubation stage is relatively low, fluctuating between 1.206×10^5 and 2.557×10^5 mv·ms. When reaching the later incubation stage, the cumulative AE energy of outburst-rockburst compound dynamic disasters is significantly greater than that of rockburst-outburst compound dynamic disasters, and the cumulative AE energy increases sharply in the early excitation stage, posing a strong risk. The cumulative AE energy growth rates in the early incubation, the later incubation, and the early excitation stages are defined as K_1, K_2, and K_3, respectively. The rockburst-outburst compound dynamic disaster K_2/K_1 value is 1.7-2.44 times, and that of K_3/K_2 is 11.12-13.7 times. The outburst-rockburst compound dynamic disaster K_2/K_1 value is 3.18-4.56 times, and the K_3/K_2 value is 6.12-6.57 times. The K_2/K_1 value is higher in outburst-rockburst compound dynamic disasters, while that of K_3/K_2 is higher in rockburst-outburst compound dynamic disasters. The cumulative AE energy of the compound dynamic disaster evolution process experiences a slow growth → rapid growth → sharp increase. Therefore, real-time monitoring of the mine working environment using acoustic emission equipment can provide early warnings of dynamic disasters.

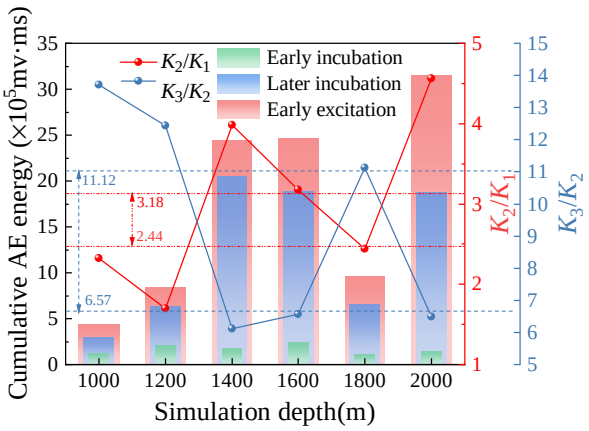

Fig. 8. Evolution of AE parameters under different simulation depths.

3.3 Evolution characteristics of coal seam temperature

In the incubation and excitation stages of compound dynamic disasters, gas will be adsorbed and desorbed, during which energy conversion takes place, accompanied by the change in coal seam temperature (Ren et al., 2024). Usually, before the disaster strikes, the coal seam temperature changes abnormally. By analyzing the coal seam temperature changes during the incubation and excitation stages of the disaster, one can explore the feasibility of predicting and preventing compound dynamic disasters based on coal seam temperature changes.

The temperature evolutions of the same type of compound dynamic disasters are similar. Due to space limitations, a set of data for each disaster is selected for analysis. Figs. 9 and 10 show the evolution curves of gas pressure and temperature with time at simulation depths of 1,200 and 2,000 m, respectively. Throughout the disaster incubation, the temperature generally shows a rising trend, with increases of 0.56∼0.94 °C and 0.88∼1.50 °C, respectively. During the gas extraction stage, there are obvious fluctuations, showing first decrease and then rise. When the gas pressure increases from 0.6 to 1.0 MPa, the coal temperature rises steadily. This is because under the action of *in-situ* stress, cracks and micro-cracks are generated in the coal body, breaking the initial adsorption equilibrium of the coal seam. At this time, as the gas pressure increases, the coal seam continues to adsorb. However, adsorption is an exothermic process, leading to a continuous increase in coal seam temperature. During gas extraction, the gas pressure gradually decreases and the adsorbed gas in the coal seam is desorbed, leading to heat loss and a fluctuating decrease in temperature. After the drainage, the gas is still desorbed and the temperature continues to decrease. In the stress disturbance stage, the adsorption rate is greater than the desorption rate, resulting in fluctuating increases in the coal seam temperature. When the disaster is excited, the temperature drops sharply, and there is a delay effect in the temperature change at the coal rock interface. This is because the transmission of temperature requires time. When the coal seam temperature decreases, there is a delay in the transmission to the coal rock interface, which is generally 1∼2 s. It can also be found that after the outburst, the temperature change in the coal seam is greater than that in the incubation stage. When the simulation depths are 1,200 and 2,000 m, the temperature changes (ΔT) are -0.99∼-1.21 °C and -1.62∼-2.27 °C, respectively.

For different positions in the coal seam, the temperature variations from T_1 to T_6 increase successively in the incubation stage and decrease successively in the excitation stage. The reason is that the air inlet is in the middle of the left side, close to T_3 and T_6. In the incubation stage, the coal seam adsorbs a large amount of gas, resulting in a temperature rise. Therefore, $\Delta T_6 > \Delta T_4$, $\Delta T_3 > \Delta T_1$. When outburst occurs, since T_1 and T_4 are close to the outburst mouth, after the outburst, the coal mass gradually destroys from the mouth to the surroundings, resulting in a decrease in coal mass temperature. As the outburst continues, the fracture network generated in the coal mass develops toward the deep part of the coal seam, providing a flow channel for the gas generated by static desorption in the deep coal seam. This makes the temperature decrease in the deep coal seam smaller than that near the outburst mouth. In addition, at the coal rock interface, there are differences in the physical and mechanical properties between the coal seam and the rock mass. Since the outburst generates shock waves towards the interior of the coal seam, when the shock waves propagate to the interface between the coal seam and the rock mass, strong transmission and reflection phenomena occur, causing the stress on the coal seam to increase exponentially. As a result, the coal mass is subjected to severe compression, and when this exceeds the bearing strength of the coal mass, the coal mass will be crushed and destroyed (Zhou et al., 2021). As such, the coal mass at this position is more severely damaged than the central position of the coal seam, resulting in more fractures, which is conducive to the migration of gas generated by desorption in the deep coal seam. At the same time, it also takes away the heat of the coal mass, leading to a larger decrease in coal mass temperature at this position compared to the central position. That is, $\Delta T_1 > \Delta T_4$, which is consistent with the previous conclusions (Ren et al., 2024), indicating the accuracy of the test.

By contrastively analyzing the temperature evolution of two different types of disasters, we can observe that the temperature evolution of six measuring points at 2,000 m are relatively consistent, which fluctuates with the changes in gas pressure and stress. However, the temperature evolution at 1,200 m is relatively abnormal, consistent with the characteristic of abnormal gas content before the occurrence of rockburst-outburst compound dynamic disasters. In addition, whether it is the incubation or the excitation, the temperature variation of outburst-rockburst compound dynamic disasters is always higher than that of rockburst-outburst compound dynamic disasters.

The evolution of temperature change in T_2 at edge of the coal seam and that in T_5 at the coal seam center under different simulation depths are shown in Fig. 11. Both ΔT_2 and ΔT_5 gradually increase with time, whereas ΔT_5 is greater than ΔT_2. At the same position, the temperature change in the outburst-rockburst compound dynamic disaster is greater than

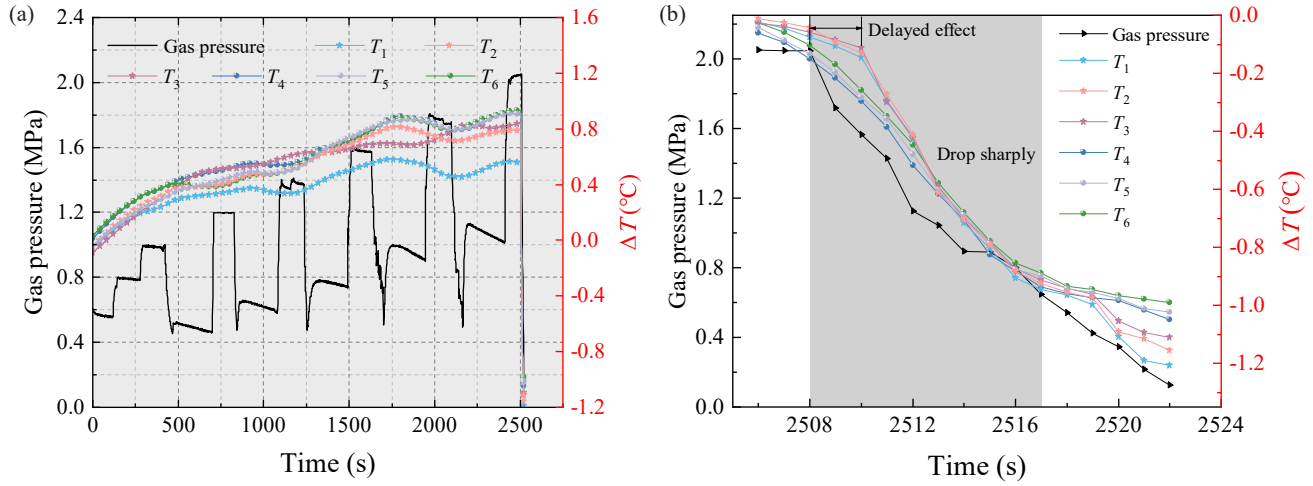

Fig. 9. Evolution of temperature and gas pressure with time at 1,200 m. (a) The entire process and (b) enlargement of excitation moment.

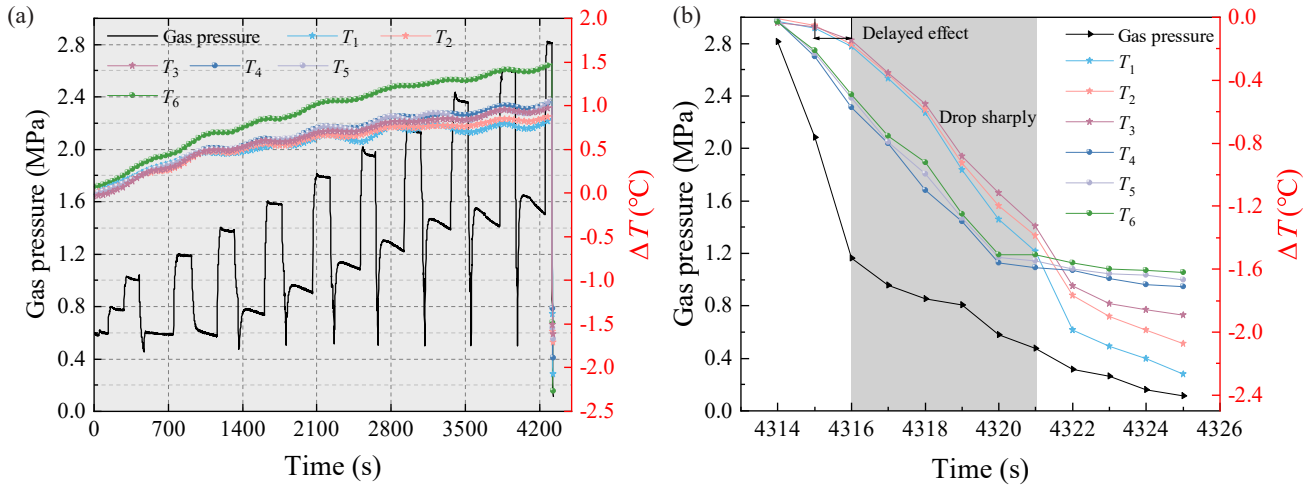

Fig. 10. Evolution of temperature and gas pressure with time at 2,000 m. (a) The entire process and (b) enlargement of excitation moment.

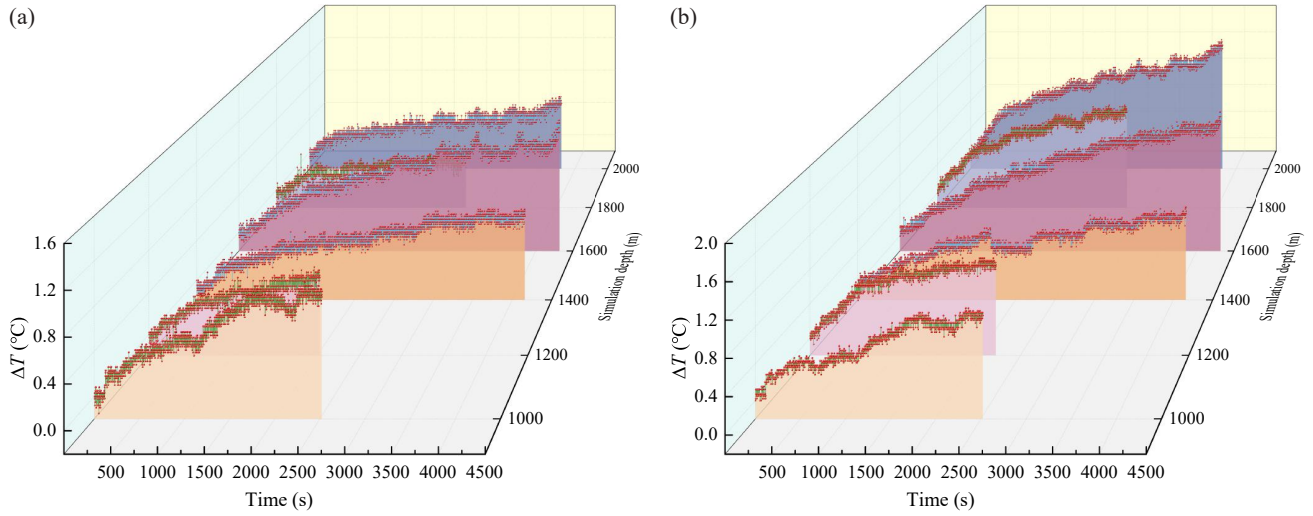

Fig. 11. Temperature variation under different simulation depths. (a) Temperature change in T_2 at the edge of coal seam and (b) temperature change in T_5 in coal seam center.

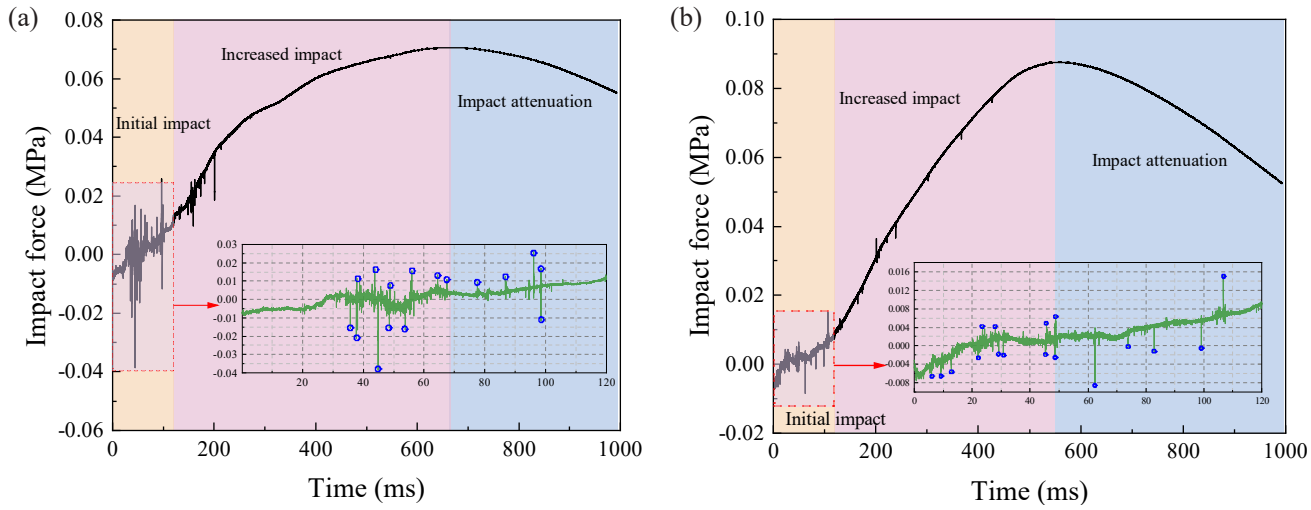

Fig. 12. Evolution of roadway impact force. (a) 1,200 m and (b) 2,000 m.

that in the rockburst-outburst compound dynamic disaster. As shown in Fig. 11, the $\Delta T_{2\max}$ of rockburst-outburst compound dynamic disaster is 0.33∼0.94 °C and the $\Delta T_{5\max}$ is 0.87∼1.16 °C, while the $\Delta T_{2\max}$ of rockburst-outburst compound dynamic disaster is 0.62∼1.1 °C, and the $\Delta T_{5\max}$ is 0.89∼1.62 °C. In the incubation stage, the coal seam gas continuously accumulates, and a large amount of free coal seam gas is stored in the coal seam through adsorption. The coal seam releases heat during the process of adsorption, causing the coal temperature to rise. Inside the coal seam, due to the small difference in the coal seam, there is no significant difference in the thermal conductivity of coal at different positions. Meanwhile, the relatively small thermal conductivity of coal is not conducive to heat dissipation, achieving the effect of heat preservation, which results in a relatively high coal temperature at the center of the coal seam. At the coal rock interface, there is a transition zone from coal to rock, where the significant difference in coal rock composition makes the coal rock mass with higher thermal conductivity more conducive to heat dissipation, ultimately leading to a significant difference in coal temperature between the edge and the center of the coal seam.

3.4 Evolution characteristics of impact force

The impact force diminishes significantly toward the far end of the roadway, often becoming negligible, while the force near the outburst mouth more accurately represents the energy released. Consequently, the impact force sensor was positioned 1,000 mm away from the outburst mouth on the roadway side. The changes in roadway impact force at various simulation depths were analyzed at this fixed measurement point, as illustrated in Fig. 12.

The evolution of the roadway impact force at 1,200 and 2,000 m are shown in Figs. 12(a) and 12(b), respectively. The findings of comparative analysis of the results of the two types of disasters are as follows:

1) For different types of compound dynamic disasters, the evolution of impact force in roadway is roughly the same. It undergoes the process of initial impact → increased impact → peak → impact attenuation, showing a peak effect. Previous studies have shown the same phenomenon (Zhang et al., 2022a). As shown in Fig. 12, violent fluctuations of the impact force occur from 0 to 120 ms, and there is negative pressure. This is because at the moment of outburst, the migration speed of the coal-gas two-phase flow is high, and the wave front squeezes the air in the roadway. In the stage of impact intensification, 1,200 and 2,000 m reach the peak points at 672.89 and 556.62 ms, respectively, with peak impact forces of 0.0706 and 0.0876 MPa, respectively. The latter growth rate of impact force is 1.69 times that of the former, indicating that the outburst-rockburst compound dynamic disaster has a strong impact airflow, resulting in greater impact destructiveness. The reason is that when outburst-rockburst compound dynamic disaster occurs, the critical gas pressure is higher and a large amount of gas expansion energy is accumulated (Zhang et al., 2022a). This energy is released suddenly, causing the impact force to rapidly increase to its peak value. Meanwhile, the rockburst-outburst compound dynamic disaster is dominated by rockburst and supplemented by outburst, and the released energy is mainly elastic deformation energy. A large amount of broken coal rock accumulates in the cavity or near the outburst mouth, and a small amount of coal rock powder is transported to the far end of the roadway under low gas pressure. Therefore, its peak impact force is smaller and the growth rate is slow.
2) The outburst process occurs intermittently and repeatedly with paroxysmal nature. According to the partial enlargement of the initial impact stage, the impact force shows irregular fluctuations for a period after the outburst is initiated, with a wide range of fluctuations, large amplitude and long duration, showing obvious turbulence characteristics. This indicates that the outburst process occurs intermittently and repeatedly with paroxysmal nature. This intermittent re-excitation process makes the outburst

show pulsating development characteristics. There are 16 and 17 main pulsating phenomena occurring at 1,200 and 2,000 m, respectively. After the occurrence of each main pulsating phenomenon, many secondary pulsating phenomena will follow. The pulsation range of the rockburst-outburst compound dynamic disaster is relatively large, and many pulsation transitions still occur in the stage of impact intensification. This is caused by abnormal gas pressure during the disaster.

The peak impact force varies with critical gas pressure and simulation depth, as shown in Fig. 13. The peak impact force in outburst-rockburst compound dynamic disaster is higher than that in rockburst-outburst compound dynamic disaster. With the increase in simulation depth, the average values of peak impact force are 0.0675, 0.0706, 0.0976, 0.0926, 0.073, and 0.0876 MPa, respectively. The impact force of different disaster types changes linearly. In this work, the critical gas pressure is divided into two intervals, $P < 2.2$ MPa and $P > 2.8$ MPa, namely outburst-rockburst and rockburst-outburst compound dynamic disasters. The piecewise fitting equation of the peak impact force and gas pressure is shown in Eq. (11). In different intervals, the peak impact force increases linearly with the critical gas pressure, and the growth rate of the peak impact force of the outburst-rockburst compound dynamic disasters is 47.76 times that of the impact-outburst compound dynamic disasters. This indicates that when the gas pressure increases to a certain value, a slight change will cause huge shock disturbance, resulting in immeasurable losses. In this study, there is a value of gas pressure between 2.2 and 2.8 MPa, which leads to the transition of disaster type from rockburst-outburst to outburst-rockburst. This is because as the gas pressure increases, the bursting liability of the coal gradually weakens, and when it reaches a certain value, the coal seam has no bursting liability and the probability of coal and gas outburst increases. That is to say, in the gas-bearing coal seam where rockburst and outburst can occur, there is a critical value of gas pressure. When the gas pressure is higher than this critical value, the outburst-rockburst compound dynamic disaster with coal and gas outburst as the main disaster occurs; when the gas pressure is lower than this critical value, the rockburst-outburst compound dynamic disaster with rockburst as the main disaster occurs. Wang et al. (2010) showed that the critical value of gas pressure for rockburst-outburst induced transformation is 2 MPa, at which point the coal seam exhibits no bursting liability. This is similar to the results obtained in this paper, indicating the reliability of the test:

$$\begin{aligned} F_1 &= 0.0134P + 0.0434,\ \mathrm{R}_1^2 = 0.8891\ (P < 2.2\ \mathrm{MPa}) \\ F_2 &= 0.64P - 1.715,\ \mathrm{R}_2^2 = 0.9329\ (P > 2.8\ \mathrm{MPa}) \end{aligned} \tag{11}$$

where F_1 and F_2 are peak impact forces, MPa; P is the gas pressure, MPa.

4. Discussion

Outburst-rockburst compound dynamic disasters mostly occur in the case shown in Fig. 14(a). For the working condition of this test, it is known that the small impact in the coal rock body leads to the generation of numerous fractures,

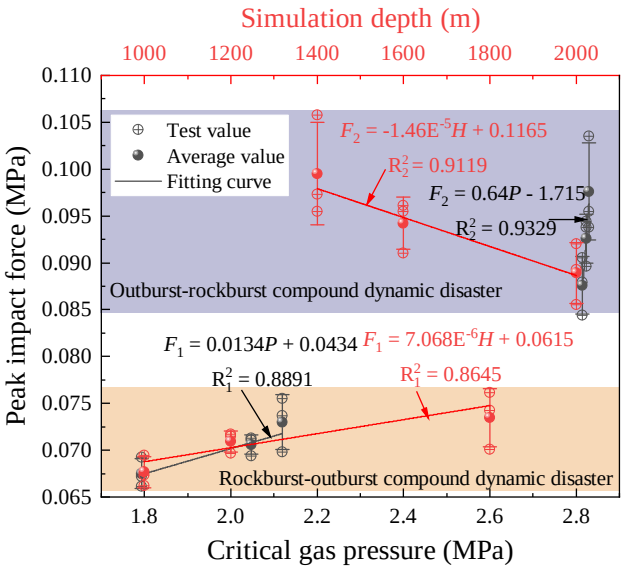

Fig. 13. Variation in peak impact force with critical gas pressure and simulation depth.

providing optimal conditions for the desorption and expansion of the gas. At the same time, the inflow of elastic energy from the outside provides the required energy conditions for the gas to release the constraints of the coal rock. The release of internal energy of gas desorption and expansion promotes the further fragmentation of the coal rock, thus providing energy and carrier for the transport of outburst material, which can induce coal and gas outburst. The several compound dynamic disasters that occurred in Pingdingshan mines No. 8, 10 and 12 belong to this kind of situation. In the second group of outburst-rockburst compound dynamic disasters, there are gas-bearing structures in the coal rock. When the impact breaks its gas overflow channel, the gas will suddenly expand and coal and gas outburst is likely to occur, as shown in Fig. 14(b). The third case outburst-rockburst compound dynamic disaster is shown in Fig. 14(c). When the coal seam floor contains rock strata with high elastic modulus, plastic failure and dilation occur at both ends of the floor under high stress conditions, while the rock strata with high elastic modulus remains intact and unplastically damaged (Zhu et al., 2018). Consequently, the dilation-induced expansion stress is applied to the high elastic modulus rock strata and generates horizontal compressive stress that tends to cause upward elastic buckling of the floor, resulting in the sealing of normal gas effusion channels in the coal rock mass. Simultaneously, the localized compression of the coal rock mass leads to the formation of cracks, reducing pore pressure and causing adsorbed gas to desorb into free gas. Once the stress borne by the floor reaches its bending strength, it leads to fracture and impact; the gas effusion channels in the compacted coal rock mass will be opened, thereby inducing coal and gas outbursts. An example of this scenario is the "7·11" compound dynamic disaster at Xinyi Coal Mine. The mechanism of roof rockburst-induced coal and gas outbursts is similar, except that the active role comes from the downward buckling of the roof.

Rockburst-outburst compound dynamic disasters predom-

Fig. 14. The incubation and occurrence process of two types of compound dynamic disasters. (a)-(c): Development and occurrence process of outburst-rockburst compound dynamic disaster, (d)-(e): Development and occurrence process of rockburst-outburst compound dynamic disaster (Zhu et al., 2018).

inantly occur in coal rock where soft and hard coals are interspersed or mutually encapsulated, as shown in Fig. 14(d). Prior to external force disturbances, the soft and hard coals constitute a relatively balanced system. Once this system encounters external disturbances such as mining or blasting, the soft coal is prone to coal and gas outbursts under the action of additional stress. The outburst of soft coal further promotes the destabilization of the entire system, potentially leading to rockbursts and thereby triggering rockburst-outburst compound dynamic disasters. This scenario is exemplified by the "11·8" compound disaster at Yangou Coal Mine. Furthermore, there is another situation when rockburst-outburst compound dynamic disasters frequently occur. During the outburst process, the ejection of fragmented coal rock masses creates a large empty roof area, which can easily induce large-scale collapse and failure of hard thick roof. This then induces roof fracture rockburst, as shown in Fig. 14(e). The results of this simulation test fall into this scenario.

At present, the prevention and control of compound dynamic disasters is crucial for safe and efficient mining in deep coal mines. Research indicates that the occurrence of compound dynamic disasters exhibits distinct stage charac-

teristics and precursor signals (Lu et al., 2020a). Prior to the occurrence of dynamic disasters, there is a long-term incubation stage and a pre-excitation stage, during which effective measures can be taken to prevent and control the disasters. For example, gas extraction can reduce the stored gas energy in coal seams, enhance the coal mass strength, and thereby decrease the probability of coal and gas outbursts as well as outburst-rockburst compound dynamic disasters (Fan et al., 2024; Jiang et al., 2024). Large-diameter drilling can increase the plastic zone of coal rock, improve coal seam permeability, and enhance the release of elastic energy, so as to control rockbursts during deep coal mining (Zhou et al., 2018b). Blasting can generate interconnected pore fracture networks, release the accumulated elastic energy in the roof-coal mass combination in advance, weaken stress concentration, and achieve the purpose of eliminating rockburst risks (Yan et al., 2015). In addition, coal seam water injections can reduce the cohesion between coal particles and friction at the particle interfaces, decrease the coal bursting liability. Meanwhile, water drives other gases, decreasing the internal energy of methane. Consequently, coal seam water injections not only release the elastic energy of coal rock but also lower the internal energy of methane, thus reducing the probability of compound dynamic disasters (Lin et al., 2023; Liang et al., 2024).

From the above analysis, it is evident that there are numerous scenarios for the occurrence of the two discussed types of compound dynamic disasters. The experiment of this study only simulated two common scenarios depicted in Figs. 14(a) and 14(e), and it was conducted on coal from a specific mine. Our next major work will focus on simulating different disaster scenarios and investigating the impact of geological or mechanical conditions of the research subject on the test results.

5. Conclusions

In this work, a new experimental method has been designed, that is, the true triaxial test that simultaneously considers gas extraction and stress loading and unloading to induce coal rock compound dynamic disasters. The effects of AE energy, temperature, and impact force during disaster incubation were evaluated to differentiate behaviors among disaster types, and the deep coal rock outburst-rockburst mutual induction and transformation mechanism was revealed. From the experimental findings, the following conclusions can be drawn:

1) Outburst-rockburst compound dynamic disasters exhibit higher relative outburst intensity and critical gas pressure compared to rockburst-outburst compound dynamic disasters. A critical gas pressure range of 2.2-2.8 MPa was identified as a threshold for disaster type transformation.
2) Deep coal rock disasters can be characterized by long incubation and short excitation, and the incubation and excitation time of the rockburst-outburst compound dynamic disaster are shorter than those of the outburst-rockburst compound dynamic disaster. The AE energy undergoes an evolution of stationary → rising → peak, with the cumulative AE energy experiencing a slow growth → rapid growth → sharp increase. The value of K_2/K_1 is higher in outburst-rockburst compound dynamic disasters, while that of K_3/K_2 is higher in rockburst-outburst compound dynamic disasters.
3) During the disaster incubation stage, temperatures generally rise, with the coal seam experiencing greater changes than the coal-rock interface. Upon excitation, temperatures drop sharply, with the coal-rock interface exhibiting more significant changes than the coal seam. Additionally, the temperature variation in outburst-rockburst compound dynamic disasters is consistently higher than in rockburst-outburst compound dynamic disasters.
4) Among different compound dynamic disasters, the evolution of impact force in roadways follows a similar pattern: Initial impact → increased impact → peak → impact attenuation, exhibiting a peak effect. The peak impact force rises linearly with critical gas pressure. Notably, the growth rate of peak impact force for outburst-rockburst compound dynamic disasters is 47.76 times that of impact-outburst compound dynamic disasters, indicating that the safety risk to coal mine production is greater.

This study explores the mechanism of mutual induction and transformation in deep coal rock compound dynamic disasters. Future work will optimize the experimental conditions, analyze various factors influencing disasters, and enhance coal mine safety. To promote the practical implementation of research findings, field tests and engineering applications will also be conducted.

Acknowledgements

This research was financially supported by the National Natural Science Foundation of China (Nos. 52374122 and 51874165), and the Liaoning Xingliao Talent Program (No. XLYC1902106).

Conflict of interest

The authors declare no competing interest.

References

Cai, M., Guo, Q., Li, Y., et al. *In situ* stress measurement and its application in the $10^{/rmth}$ Mine of Pingdingshan Coal Group. Journal of University of Science and Technology Beijing, 2013, 35(11): 1399-1406. (in Chinese)

Cao, J., Sun, H., Wang, B., et al. A novel large-scale three-dimensional apparatus to study mechanisms of coal and gas outburst. International Journal of Rock Mechanics and Mining Sciences, 2019, 118: 52-62.

Chen, H., Qi, H., Long, R., et al. Research on 10-year tendency of China coal mine accidents and the characteristics of human factors. Safety Science, 2012, 50(4): 745-750.

Díaz Aguado, M. B., González Nicieza, C. Control and pre-

vention of gas outbursts in coal mines, Riosa-Olloniego coalfield, Spain. International Journal of Coal Geology, 2007, 69(4): 253-266.

Dong, G., Liang, X., Wang, Z. The properties of a coal body and prediction of compound coal-rock dynamic disasters. Shock and Vibration, 2020, 2020: 8830371.

Dou, L., Mu, Z., Li, Z., et al. Research progress of monitoring, forecasting, and prevention of rockburst in underground coal mining in China. International Journal of Coal Science & Technology, 2014, 1(3): 278-288.

Fan, C., Sun, H., Li, S., et al. Research advances in enhanced coal seam gas extraction by controllable shock wave fracturing. International Journal of Coal Science & Technology, 2024, 11: 39.

Geng, J., Nie, W., Yang, S., et al. Experimental study on dynamic evolution mechanism during coal and gas outburst. IOP Conference Series: Earth and Environmental Science, 2020, 570(4): 042027.

Hu, Q., Zhang, S., Wen, G., et al. Coal-like material for coal and gas outburst simulation tests. International Journal of Rock Mechanics and Mining Sciences, 2015, 74: 151-156.

Jiang, J., Deng, Z., Zhang, G., et al. A case study for coupling mechanism of anti-rockburst and pressure relief in gas drainage borehole along seam. Frontiers in Earth Science, 2024, 12: 1354238.

Jiang, Y., Wang, H., Xue, S., et al. Assessment and mitigation of coal bump risk during extraction of an island longwall panel. International Journal of Coal Geology, 2012, 95: 20-33.

Jin, K., Cheng, Y., Ren, T., et al. Experimental investigation on the formation and transport mechanism of outburst coal-gas flow: Implications for the role of gas desorption in the development stage of outburst. International Journal of Coal Geology, 2018, 194: 45-58.

Konicek, P., Soucek, K., Stas, L., et al. Long-hole destress blasting for rockburst control during deep underground coal mining. International Journal of Rock Mechanics and Mining Sciences, 2013, 61: 141-153.

Liang, Y., Shi, B., Yue, J., et al. Anisotropic damage mechanism of coal seam water injection with multiphase coupling. ACS Omega, 2024, 9(14): 16400-16410.

Li, B., Wang, E., Li, Z., et al. Automatic recognition of effective and interference signals based on machine learning: A case study of acoustic emission and electromagnetic radiation. International Journal of Rock Mechanics and Mining Sciences, 2023, 170: 105505.

Li, T., Cai, M., Cai, M. A review of mining-induced seismicity in China. International Journal of Rock Mechanics and Mining Sciences, 2007, 44(8): 1149-1171.

Li, X., Chen, S., Wang, E., et al. Rockburst mechanism in coal rock with structural surface and the microseismic (MS) and electromagnetic radiation (EMR) response. Engineering Failure Analysis, 2021, 124(3): 105396.

Li, Z., Wang, E., Ou, J., et al. Hazard evaluation of coal and gas outbursts in a coal-mine roadway based on logistic regression model. International Journal of Rock Mechanics and Mining Sciences, 2015, 80: 185-195.

Lin, X., Liu, Z., Geng, N., et al. Optimization and application of water injection process in gas-bearing coal seam. Processes, 2023, 11(10): 3003.

Lu, J., Yin, G., Gao, H., et al. True triaxial experimental study of disturbed compound dynamic disaster in deep underground coal mine. Rock Mechanics and Rock Engineering, 2020a, 53(5): 2347-2364.

Lu, J., Zhang, D., Huang, G., et al. Effects of loading rate on the compound dynamic disaster in deep underground coal mine under true triaxial stress. International Journal of Rock Mechanics and Mining Sciences, 2020b, 134: 104453.

Nie, B., Ma, Y., Hu, S., et al. Laboratory study phenomenon of coal and gas outburst based on a mid-scale simulation system. Scientific Reports, 2019, 9(1): 15005.

Pan, Y., Song, Y., Luo, H., et al. Coalbursts in China: Theory, practice and management. Journal of Rock Mechanics and Geotechnical Engineering, 2024, 16(1): 1-25.

Petukhov, I. Rock Burst in Coal Mine. Beijing, China, China Coal Industry Press, 1983.

Qiu, L., Zhu, Y., Liu, Q., et al. Response law and indicator selection of seismic wave velocity for coal seam outburst risk. Advances in Geo-Energy Research, 2023, 9(3): 198-210.

Ren, L., Tang, J., Pan, Y., et al. A new risk indicator of outburst based on coal-seam temperature variation and acoustic emission signal. Rock Mechanics and Rock Engineering, 2024, 58(2): 1739-1755.

Shepherd, J., Rixon, L., Griffiths, L. Outbursts and geological structures in coal mines: A review. International Journal of Rock Mechanics and Mining Sciences & Geomechanics Abstracts, 1981, 18(4): 267-283.

Skoczylas, N. Laboratory study of the phenomenon of methane and coal outburst. International Journal of Rock Mechanics and Mining Sciences, 2012, 55: 102-107.

Skoczylas, N., Dutka, B., Sobczyk, J. Mechanical and gaseous properties of coal briquettes in terms of outburst risk. Fuel, 2014, 134: 45-52.

Sobczyk, J. The influence of sorption processes on gas stresses leading to the coal and gas outburst in the laboratory conditions. Fuel, 2011, 90(3): 1018-1023.

Sobczyk, J. A comparison of the influence of adsorbed gases on gas stresses leading to coal and gas outburst. Fuel, 2014, 115: 288-294.

Soleimani, F., Si, G., Roshan, H., et al. Numerical modelling of coal and gas outburst initiation using energy balance principles. Fuel, 2023, 334: 126687.

Tang, J., Zhang, X., Sun, S., et al. Evolution characteristics of precursor information of coal and gas outburst in deep rock cross-cut coal uncovering. International Journal of Coal Science & Technology, 2022, 9: 5.

Wang, C., Liu, Y., Song, D., et al. Evaluation of bedding effect on the bursting liability of coal and coal-rock combination under different bedding dip angles. Advances in Geo-Energy Research, 2024, 11(1): 29-40.

Wang, C., Yang, S., Yang, D., et al. Experimental analysis of the intensity and evolution of coal and gas outbursts. Fuel, 2018, 226: 252-262.

Wang, J., Jiang, F., Meng, X., et al. Mechanism of rock burst occurrence in specially thick coal seam with rock parting. Rock Mechanics and Rock Engineering, 2016, 49(5): 1953-1965.

Wang, K., Du, F. The classification and mechanisms of coal-gas compound dynamic disasters: A preliminary discussion. International Journal of Mining and Mineral Engineering, 2019, 10(1): 68-84.

Wang, X., Tian, C., Wang, Q., et al. Study on influencing factors and prevention measures of coal-rock-gas compound dynamic disaster in deep coal mine mining. Scientific Reports, 2025, 15(1): 2080.

Wang, Z., Yin, G., Hu, Q., et al. Inducing and transforming conditions from rockburst to coal-gas outburst in a high gassy coal seam. Journal of Mining & Safety Engineering, 2010, 27(4): 572-575+580. (in Chinese)

Wei, C., Zhang, C., Canbulat, I., et al. Evaluation of current coal burst control techniques and development of a coal burst management framework. Tunnelling and Underground Space Technology, 2018, 81: 129-143.

Xie, H., Gao, M., Zhang, R., et al. Study on the mechanical properties and mechanical response of coal mining at 1,000 m or deeper. Rock Mechanics and Rock Engineering, 2019, 52(5): 1475-1490.

Xu, L., Jiang, C. Initial desorption characterization of methane and carbon dioxide in coal and its influence on coal and gas outburst risk. Fuel, 2017, 203: 700-706.

Xue, S., Wang, Y., Xie, J., et al. A coupled approach to simulate initiation of outbursts of coal and gas-Model development. International Journal of Coal Geology, 2011, 86(2): 222-230.

Xue, Y., Gao, F., Teng, T., et al. Effect of gas pressure on rock burst proneness indexes and energy dissipation of coal samples. Geotechnical and Geological Engineering, 2016, 34(6): 1737-1748.

Yang, D., Chen, Y., Tang, J., et al. Comparative experimental study of methods to predict outburst risk when uncovering coal in crosscuts. Fuel, 2021, 288: 119851.

Yang, W., Lu, C., Lin, B., et al. Tunnelling outburst potential affected by mechanical properties of coal seam. Tunnelling and Underground Space Technology, 2019, 83(1): 99-112.

Yan, P., Zhao, Z., Lu, W., et al. Mitigation of rock burst events by blasting techniques during deep-tunnel excavation. Engineering Geology, 2015, 188: 126-136.

Yuan, L. Control of coal and gas outbursts in Huainan mines in China: A review. Journal of Rock Mechanics and Geotechnical Engineering, 2016, 8(4): 559-567.

Zhang, C., Wang, E., Xu, J., et al. A new method for coal and gas outburst prediction and prevention based on the fragmentation of ejected coal. Fuel, 2021, 287: 119493.

Zhang, M., Xu, Z., Pan, Y., et al. A united instability theory on coal (rock) burst and outburst. Journal of China Coal Society, 1991, 16(4): 48-52. (in Chinese)

Zhang, X., Tang, J., Pan, Y., et al. Experimental study on intensity and energy evolution of deep coal and gas outburst. Fuel, 2022a, 324: 124484.

Zhang, X., Tang, J., Yu, H., et al. Gas pressure evolution characteristics of deep true triaxial coal and gas outburst based on acoustic emission monitoring. Scientific Reports, 2022b, 12(1): 21738.

Zhang, Z., Xie, H., Zhang, R., et al. Deformation damage and energy evolution characteristics of coal at different depths. Rock Mechanics and Rock Engineering, 2019, 52(5): 1491-1503.

Zhao, Y., Jiang, Y. Acoustic emission and thermal infrared precursors associated with bump-prone coal failure. International Journal of Coal Geology, 2010, 83(1): 11-20.

Zhou, A., Wang, K., Feng, T., et al. Effects of fast-desorbed gas on the propagation characteristics of outburst shock waves and gas flows in underground roadways. Process Safety and Environmental Protection, 2018a, 119: 295-303.

Zhou, A., Zhang, M., Wang, K., et al. Rapid gas desorption and its impact on gas-coal outbursts as two-phase flows. Process Safety and Environmental Protection, 2021, 150: 478-488.

Zhou, B., Xu, J., Peng, S., et al. Test system for the visualization of dynamic disasters and its application to coal and gas outburst. International Journal of Rock Mechanics and Mining Sciences, 2019, 122(10): 104038.

Zhou, H., Gao, J., Han, K., et al. Permeability enhancements of borehole outburst cavitation in outburst-prone coal seams. International Journal of Rock Mechanics and Mining Sciences, 2018b, 111: 12-20.

Zhu, L., Pan, Y., Li, Z., et al. Mechanisms of rockburst and outburst compound disaster in deep mine. Journal of China Coal Society 2018, 43(11): 3042-3050. (in Chinese)